Calculations of Capacitive Couplings in Induction Generators to Analyse Shaft Voltage

*Jafar Adabi, *Firuz Zare, *Arindam Ghosh, **Robert D. Lorenz,

*School of Electrical Engineering
Queensland University of Technology
GPO Box 2434, Brisbane, Australia
adabi.jafar@student.qut.edu.au

**University of Wisconsin-Madison
Depts. of ME and ECE
1513 University Avenue, Madison, USA
lorenz@engr.wisc.edu

Abstract

This paper deals with the analysis of the parameters which are effective in shaft voltage generation of induction generators. It focuses on different parasitic capacitive couplings by mathematical equations, finite element simulations and experiments. The effects of different design parameters have been studied on proposed capacitances and resultant shaft voltage. Some parameters can change proposed capacitive coupling such as: stator slot tooth, the gap between slot tooth and winding, and the height of the slot tooth, as well as the air gap between the rotor and the stator. This analysis can be used in a primary stage of a generator design to reduce motor shaft voltage and avoid additional costs of resultant bearing current mitigation.

1. Introduction

Pulse width modulated inverters are widely used in industrial and commercial applications due to the growing need of speed control in adjustable speed motor drive systems. This voltage, generated by an inverter, is a major cause of bearing failures in a motor drive system. All inverters generate a common mode voltage relative to the ground, which creates a shaft voltage due to parasitic capacitances in the motor. This occurrence can cause many unwanted problems in the interaction with parasitic capacitive couplings in an AC motor [1-3]. Common mode voltage generated by a PWM inverter in AC motor drive systems can cause shaft voltage and resultant bearing currents due to capacitive coupling between winding, stator and rotor [4-5].

Different approaches and techniques have been proposed in [4, 8] to calculate capacitive coupling in AC motors and to extract high frequency parameters of an AC motor for EMI analysis. In [6-7], different types of techniques to measure shaft voltage and bearing current in motor drive systems have been discussed. Active EMI filter using an extra leg in an inverter to cancel zero voltage vectors have been proposed in [9]. Common mode voltage and shaft voltage in a doubly fed induction generator (DFIG) and their reduction techniques have been discussed in [10-12]. In these papers, the effect of PWM voltage from both stator and rotor sides have been considered and methods for shaft voltage reduction have been investigated.

This paper focuses on the design parameters of a stator slot which are effective in high frequency analysis. A detailed mathematical analysis will be carried out to determine the effects of these parameters on motor shaft voltage. Fig. 1 (a

and b) show the structures of an stator-fed induction generator (IG) and a DFIG where the parasitic capacitive couplings exist between: the stator winding and rotor (C_{sr}), the stator winding and stator frame (C_{sf}), the rotor and stator frames (C_{rf}), stator winding and rotor winding (C_{ws}), the rotor winding and rotor (C_{wr}), rotor winding and stator frame (C_{wf}) and ball bearing and outer and inner races (C_{BO}, C_{BI}).

Common mode voltage creates the shaft voltage through electrostatic couplings. A simple high frequency model of IG is shown in Fig. 1 (c), from which the shaft voltage can be calculated as:

$$V_{shaft} = \frac{C_{sr}}{C_b + C_{rf} + C_{sr}} \times V_{com} \tag{1}$$

The main issues regarding the operation of power converters used in DFIG structures are common mode voltage from both rotor and stator side converters. According to Fig. 1 (d), the shaft voltage in a DFIG can be calculated as:

$$V_{shaft} = \frac{C_{wr}}{C_{wr} + C_{rf} + C_b + C_{sr}} \times V_{com,R} + \frac{C_{sr}}{C_{wr} + C_{rf} + C_b + C_{sr}} \times V_{com,S} = K_R \times V_{com,R} + K_S \times V_{com,S} \tag{2}$$

where $V_{com,R}$ and $V_{com,S}$ are the common mode voltages from the rotor and stator windings, respectively. K_R and K_S are respectively defined as rotor and stator side capacitance factors which are effective in total shaft voltage generation.

The main goal of this work is to find the effect of machine parameters on the shaft voltage and to use a model to analyse of this effect. In this research, a mathematical equation has been developed to calculate the shaft voltage in induction generators with respect to various design parameters.

2. Calculation of shaft voltage and relevant capacitive couplings in a motor structure

Fig. 2 (a) shows a view of a stator slot, a rotor and its winding where g_1 is the air gap between rotor and stator, g_2 is the gap between winding and stator, g_{in} is the thickness of the winding insulation, d is the length of slot tooth and ρ is the height of the stator slot. W and W′ are the width of winding at the top and bottom respectively, h_W is the length of the stator winding at both the right and the left sides. Following capacitive couplings can be calculated that are present in the structure of induction generators.

2.1. The capacitive coupling between rotor and frame (C_{rf})

By considering the air gap (g_1) to be much smaller than the outer diameter of the rotor, a capacitive coupling between rotor and stator frame in a single stator slot can be calculated as follows:

$$C_{rf} = \frac{\varepsilon_0 (\frac{2\pi r}{n} - d) \times L_r}{g_1} \tag{3}$$

where r is the rotor radius and g_1 is the air gap, L_r is the rotor length. This capacitance can be multiplied by the number of slots (n) to calculate the total capacitance.

2.2. The capacitive coupling between frame and stator winding (C_{sf})

In this case, there are four surfaces which surround the winding. So, C_{sf} can be calculated as:

$$C_{sf} = \frac{\varepsilon_0 \varepsilon_r (W' + 2 \times h_W) \times L_r}{g_{in}} + C_{top} \tag{4}$$

where C_{top} is the capacitance between the upper side of winding and the stator slot tooth. This capacitance consists of insulation capacitance ($C_{in,top}$) and slot wedge capacitance (C_{wedge}), where:

$$C_{in,top} = \frac{\varepsilon_0 \varepsilon_{r1} (W - d) \times L_r}{g_{in}} \quad , C_{wedge} = \frac{\varepsilon_0 \varepsilon_{r2} (W - d) \times L_r}{g_2} \tag{5}$$

Therefore, C_{top} can be calculated as:

$$C_{top} = \frac{C_{in,top} \times C_{wedge}}{C_{in,top} + C_{wedge}} = \frac{\varepsilon_0 \varepsilon_{r1} \varepsilon_{r2} (W - d) \times L_r}{g_2 \varepsilon_{r1} + g_{in} \varepsilon_{r2}} \tag{6}$$

Based on these calculations, the capacitance between winding and stator frame is:

$$C_{sf} = \left(\frac{\varepsilon_0 \varepsilon_r (W' + 2 \times h_W)}{g_{in}} + \frac{\varepsilon_0 \varepsilon_{r1} \varepsilon_{r2} (W - d)}{g_2 \varepsilon_{r1} + g_{in} \varepsilon_{r2}} \right) \times L_r \tag{7}$$

where ε_0 is the permittivity of free space and ε_{r1}, ε_{r2} are the permittivity of the insulation and the slot wedge material.

2.3. The capacitive coupling between ball bearings and inner and outer races

Fig. 2 (b) shows the sketch of the ball bearing in the AC generator and the schematic of two capacitances of a ball bearing. Calculation of ball bearing capacitances is not an easy task because the geometrical structure is rather complex [1]. Previous different approaches have been used to calculate these capacitive couplings [6-8]. As shown in Fig. 2 (b) that there are balls between the outer and the inner races with lubricating grease between the balls and the races. There are capacitive couplings between ball bearings and the outer and inner races (C_{BO} and C_{BI}). The ball bearing capacitance is calculated by:

$$C_B = \frac{1}{\frac{1}{C_{BI}} + \frac{1}{C_{BO}}} \tag{8}$$

2.4. The capacitive coupling between rotor and stator winding (C_{sr})

As shown in Fig. 3 (a), existing capacitive couplings are: the capacitive coupling between rotor and winding (C_{sr}), the capacitive coupling between rotor and stator in left and right sides of the slot tooth (C_{f1r}, C_{f2r}), and capacitive coupling between winding and stator in left and right sides of the slot tooth ($C_{f1s,}$ C_{f2s}). Fig.3 (b) shows a model than is proposed to calculate the capacitive couplings. In fact, the electric fields between stator slot teeth on both sides influence the total electric field between the rotor and stator. Fig. 3 (c) shows a typical electric field in the proposed system (the voltages applied to upper, lower and besides objects are 50, 100 and 0 volts respectively). To calculate the side capacitances (C_{f1r}, C_{f2r}, $C_{f1s,}$ C_{f2s}), the structure of two surfaces with the voltage difference of V_0 and the angle of φ (here $\varphi = 90^0$)

needs to be considered. As shown in Fig. 3 (d), the small gap between two surfaces is ρ_1 and the length of the surface is ρ_2. The capacitance can be calculated as:

$$C = \frac{Q}{V} = \frac{\varepsilon_0 \int E.dS}{V} \tag{9}$$

Based on [13], the electric field between two surfaces can be calculated by:

$$E = -\nabla V = -\frac{1}{\rho}\frac{dV}{d\varphi}\overrightarrow{a_\varphi} = -\frac{V_0}{\rho\varphi_0}\overrightarrow{a_\varphi} \tag{10}$$

Considering $ds = d\rho\, dz\, \overrightarrow{a_\varphi}$ in cylindrical coordinates, the capacitive coupling between two surfaces is:

$$C = \frac{\varepsilon_0 \int_{\rho_1}^{\rho_2}\int_0^d \frac{V_0}{\rho\varphi_0} d\rho\, dz\, \overrightarrow{a_\varphi}}{\frac{V_0}{\varphi_0}\varphi} = \frac{\varepsilon_0 \frac{V_0 t}{\varphi_0} Ln\left(\frac{\rho_2+\rho_1}{\rho_1}\right)}{\frac{V_0}{\varphi_0}\varphi} = \frac{\varepsilon_0 t}{\varphi} Ln\left(\frac{\rho_2+\rho_1}{\rho_1}\right) \tag{11}$$

Because of a small gap between the two surfaces, the system model in Fig. 3 (b) can be simplified as in Fig. 3 (c). Thus, the electric field between half of f_1 and the rotor can create a capacitive coupling C_{f1r} and another half of f_1 can create the capacitive coupling with stator winding (C_{f1s}). The same is also found in the other side of the stator slot tooth (f_2) and resultant capacitive couplings (C_{f2r}, C_{f2s}). According to Eq. 10, these capacitances are:

$$\begin{cases} C_{f1r} = C_{f2r} = \frac{2\varepsilon_0}{\pi} Ln\left(\frac{\rho/2 + g_1}{g_1}\right) \\ C_{f1s} = C_{f2s} = \frac{2\varepsilon_0}{\pi} Ln\left(\frac{\rho/2 + g_2}{g_2}\right) \end{cases} \tag{12}$$

Considering the electric field between sides of the slot tooth (S_1, S_2), the effective area to calculate capacitive couplings between rotor and stator will decrease and C_{sr} is:

$$C_{sr} = \varepsilon_0 \frac{d-\rho}{\rho + g_1 + g_2} \tag{13}$$

Fig.4 shows the error between simulations and calculations of C_{sr} in a complete system model versus a variation of g_2 (ρ=5, 25 mm and g_1=1, 2 mm) over a wide rage of stator slot tooth (d).

3. Simulation Results

Capacitance matrices of multi-conductor systems in different 3-D model designs of the motor have been extracted by simulation [14] and compared with the 2-D simulation analysis and the calculation results. Also, a simulation study for ball bearing capacitances was carried out for different conditions.

3.1. Effects of the parameters of stator slot on different capacitive couplings

Rotor radius=1000mm: In this section, simulations were conducted for a single slot for 12 design structures of Table I. The thickness of insulation (g_{in}) is considered as 2.5 mm and ε_r is 2.25. Fig. 5. (a-c) show the calculated, 2-D, 3-D

results in single stator slot for C_{sr}, $C_{rf,}$ C_{sf} respectively. In a 3-D analysis, fringing effects at the both sides of the stator have been considered while in 2-D analysis, it is not possible to consider these effects. A complete generator system (number of slots=24) has been simulated based on the first six designs of Table I (see Fig.5 d and e) using 3-D analysis.

Table I. different design parameters for IG structure

Design number	ρ (mm)	g_2 (mm)	d (mm)	w (mm)	h_w (mm)
1	3	5	50	200	289
2	5	5	50	200	287
3	3	15	50	201	278
4	5	15	50	201	276
5	3	25	50	203	268
6	5	25	50	205	266
7	3	5	150	200	289
8	5	5	150	200	287
9	3	15	150	201	278
10	5	15	150	201	276
11	3	25	150	203	268
12	5	25	150	205	266

Rotor radius=600mm: A simulation study has been carried out for a single stator slot with the design parameters of Table II. Fig. (6) shows the variation of C_{sf} versus the changes of g_2 where g_1=1mm, d=8, ρ=4mm. It shows that by changing g_2 from 5 to 50 mm, C_{sf} changes between 4.88nF and 4.04 nF, which is not a big variation. Fig.6 (b) shows the variation of C_{sf} versus stator slot tooth and two different air gaps. It can be seen that the effects of the stator slot tooth on C_{sf} are very low. Fig. 6 (c) shows the changes of C_{sr} versus stator slot tooth at two different air gaps. It shows slot tooth variation has a great effect on this capacitance while the air gap is not an effective factor. As shown in Fig.6 (d), the capacitance decreases with increments of the stator slot tooth.

Table II. Different design parameters of a single slot

Rotor radius	600 mm
Stator Slot tooth(d)	8, 16,24,32,40 mm
Air gap (g_1)	1, 1.5 mm
Gap between slot tooth and winding (g_2)	5,10,15,…,50 mm
Height of slot tooth (ρ)	4,8,12 mm

3.2. Analysis of ball bearing capacitances in different conditions

During operation, the changes in the distances between the balls and races may change and vary the capacitance. At high speed, balls and shaft positions are considered symmetric and the distances between the inner race and balls (d_{BI}) and between outer races and balls (d_{BO}) are assumed to be equal. Also the shaft position is not changed and the shaft and outer race is concentric (see Fig.2). At low speeds, because of gravity, balls and shaft may shift down and the system (balls position and shaft) will be asymmetrical. As shown in Fig.7 (a), in this asymmetric case, the upper and lower side balls are shifted down because of gravity but the separations between the inner and outer races with other is approximately symmetrical.

As shown as in Fig.7 (b), at lower speeds, an asymmetric shaft position may occur, which is more common than other cases. In this simulation, there are 22 balls with a diameter of 30 mm, a shaft diameter of 200 mm and the range of

0.1mm oil thickness was simulated. The shaft position is shifted down corresponding to 20%, 40% and 60% grease thickness. Table III shows the capacitive coupling terms (C_{BO}, C_{BI}) with respect to different variables associated with the balls position assuming equal inner and outer distances.

Table III. Capacitive coupling terms in different ball position

Oil Thickness (mm)	d_{BO} (mm)	d_{BI} (mm)	C_{BO} (pF)	C_{BI} (pF)	C_B (pF)
0. 1	0.01	0.09	363	78.393	64.47
0. 1	0.03	0.07	173.91	88.01	58.43
0. 1	0.05	0.05	130.07	104.44	57.927
0. 1	0.07	0.03	108.09	132.93	59.614
0. 1	0.09	0.01	94.275	216.14	65.64
Shaft centre shift down (mm)	d_{BO} (mm)	d_{BI} (mm)	C_{BO} (pF)	C_{BI} (pF)	C_B (pF)
0.02	0.04	0.04	145.84	116.17	64.662
0.04	0.03	0.03	172.07	132.92	74.991
0.06	0.02	0.02	220.54	159.95	92.710

According to Fig.1 (d), in the high frequency model of the system, C_b is in parallel with the C_{rf}. C_{rf} is a big capacitance compared with bearing capacitances. Therefore, it has less effect than other capacitances. That means the value of the capacitance cannot change the shaft voltage significantly. Therefore $C_{rf}+C_b$ approximately equals to C_{rf}.

4. Experimental Results

To verify the analysis and simulation results, several tests have been performed to measure common mode and shaft voltages and compare them with the simulation results. It is very important to consider practical issues when we compare test and simulation results. Thus, simulations have been performed for a 5 kW 3-phase induction machine with 36 slots considering practical issues. In a real machine, in each slot a distance between a winding and the rotor surface (referring to Fig. 2 a, the length of $g_1+\rho+g_2$) is changed along the rotor axis and in different slots. Based on our measurement, this distance varies between (3.5 mm and 4.5 mm). Several simulations have been carried out to extract the capacitive couplings for three different distances ($g_1+\rho+g_2$), 3.5mm, 4mm and 4.5mm and the results are given in Table IV.

Table IV. Simulation results with and without end-winding (pF)

	g (mm)	C_{sr} (ε_r =2)	C_{sr} (ε_r =2.5)	C_{sr} (ε_r =3)	C_{sr} (ε_r ={2-3})	C_{rf}	V_{sh}/V_{com}
without end winding	4.5	7.1	7.2	7.2	7.2	545	0.013
	4	**10.01**	**10.05**	**10.08**	**10.05**	**545**	**0.018**
	3.5	13.22	13.32	13.35	13.29	545	0.024
with end winding	4.5	15.71	15.72	15.72	15.72	545	0.028
	4	**18.62**	**18.66**	**18.69**	**18.66**	**545**	**0.033**
	3.5	21.83	21.93	21.96	21.90	545	0.038

Another practical issue is the effect the insulator property (ε_r) on C_{sr}, which has been analysed and addressed in Eq. 14. Considering three different ε_r (2, 2.5 and 3) and also based on Fig.3(a), the capacitive coupling between the winding and the rotor can be defined as follows:

$$\frac{C_{sr\_air} \times C_{sr\_in}}{C_{sr\_air} + C_{sr\_in}} \approx C_{sr\_air} \tag{14}$$

In fact, two capacitors, C_{sr_air} and C_{sr_in} are in series and because the thickness of the insulator is much less than $(g_1+\rho+g_2)$, $C_{sr\_air} << C_{sr\_in}$ and the capacitive coupling between the winding and the rotor approximately equals to C_{sr_air}. This analysis shows that the simulations to extract the capacitive coupling between the winding and the rotor are not affected by the insulator property (ε_r). The simulation results for different ε_r (2, 2.5 and 3) are given in Table IV. According to the above discussion and based on the simulation results, the effect ε_r on C_{sr} is negligible while the effect of $(g_1+\rho+g_2)$ on C_{sr} is significant. The last practical issue is the effect of end winding on the shaft voltage. As shown in Fig.8(a), due to a capacitive coupling between the end winding and the rotor side, C_{sr_end}, the total capacitive coupling between the windings and the rotor, C_{sr_total} is increased. In a real machine, the length of the end winding and also its configuration at both sides are not uniform. To analyse this issue, each end winding has been modelled as a cylinder connected to each side of the winding as shown in Fig.8. In this induction machine, the length of the end winding varies between 30mm and 40mm and simulation results show that C_{sr_end} are 8.20 pF and 9.03 pF, respectively. Thus we have considered 8.61 pF an average of the capacitive coupling between the end windings and the rotor. According to the simulation results and based on Eq.15, V_{sh}/V_{com} ratios have been calculated for different cases and the results are given in Table IV. Eq.15 shows that the voltage ratio, V_{sh}/V_{com} approximately equals to C_{sr}/C_{rf}. Thus measuring the common mode and shaft voltages can give C_{sr}/C_{rf} ratio for the given induction machine.

$$\frac{V_{sh}}{V_{com}} = \frac{C_{sr}}{C_b + C_{sr} + C_{rf}} \approx \frac{C_{sr}}{C_{sr} + C_{rf}} \approx \frac{C_{sr}}{C_{rf}} \tag{15}$$

We have performed two main tests for the induction machine; in the first test, all capacitive couplings have been considered without shielding any part of the end winding and the results can be compared with the simulation result (with end winding). In the second test, we have shielded the end windings to compare the test result with the simulation result (without end winding). The common mode and shaft voltage waveforms with and without shielded end windings are shown in Fig.9. V_{sh}/V_{com} ratios have been calculated based on the measurement results which are given in Table V.

Table V: Comparison between the simulation and test results

	V_{sh}/V_{com}
Simulation, without end winding $g_1+\rho+g_2 = 4$ mm	0.018
Simulation, with end winding $g_1+\rho+g_2 = 4$ mm	0.033
Test results (with shielded end winding) $V_{com} = 505$ Volts, $V_{sh} = 10.5$ Volts	0.0207
Test results (without shielded end winding) $V_{com} = 505$ Volts, $V_{sh} = 15.5$ Volts	0.0306

Considering an average of 4mm for the distance between the windings and the rotor $(g_1+\rho+g_2)$, the error between the simulation result without end winding (0.018) and the test result with shielded end winding (0.0207) is around 13%. According to Eq.15, V_{sh}/V_{com} significantly depends on C_{sr} and C_{rf}. Thus, the error between the simulation and test

results are due to the variation of (g_1+ρ +g_2) values which affects C_{sr}. In the other test, we have considered the end winding effect and the error between the simulation result with end winding (0.033) and the test result without shielded end winding (0.0306) is around 8%. This error can also be addressed to capacitive couplings between the rotor and the shielded surfaces which have been grounded on both sides of the rotor (8.61 pF) and also due to a capacitive coupling between the rotor shaft and the motor frame which has not been considered in this analysis. Thus, the small error between the test and simulation results shows that this analysis and finite element simulation approach can be used as a good design tool for Induction Machine Design to analyse and reduce shaft voltage.

5. Discussion

Stator-fed induction generator: Based on the simulation results and the analysis in [7-8], in a variety of design parameters changes, the ratio between C_{sr} and C_{rf} is between 0.05 and 0.1. Also, the ratio between C_b and C_{sr} (α) is almost equal to 1. β is defined as the ratio between end-winding C_{sr} and without end-winding C_{sr}. So, $C_{sr\text{-}total}$ is (1+β) times of C_{sr} without end-winding which is calculated in Eq.13. By substituting equations 3&13 in Eq.1, the ratio between shaft voltage and common mode voltage can be written as:

$$\frac{V_{sh}}{V_{com}} \approx \frac{g_1(1+\beta)(d-\rho)}{g_1(1+\alpha)(1+\beta)(d-\rho)+(\rho+g_1+g_2)(\frac{2\pi r}{n}-d)} \quad , d>\rho \tag{16}$$

As shown in this equation, the effective parameters on shaft voltage are d, ρ, g_1 and g_2 and β. It is clear that g_1 can not be changed for a large range of variation and can not be an effective parameter in shaft voltage reduction. Fig.10(a) shows the variation of V_{sh}/V_{com} versus variation of d and g_2 where the stator slot height of ρ=5 mm. This graph shows the effect of two main design parameters on shaft voltage. According to simulation results in different parameters:

- C_{sr} is an important capacitance in case of shaft voltage generation in an IG because it can be changed by variation of the design parameters (see Fig.5 and 6) while other capacitances has not such a freedom to change.
- An increment of stator slot tooth increases the shaft voltage while increasing the gap between the slot tooth and winding decreasing the shaft voltage (see Fig.10.a). This information can be taken into account in the design procedure of the motor structure and the motor designer can choose design parameters which are a trade off between shaft voltage issue and other electromechanical considerations.

Doubly-fed induction generator: If the rotor slot shape in a DFIG is considered same as the stator slot in Fig.2, the shaft voltage in DFIG is calculated based on Eq.2 as $V_{shaft} = K_R\, V_{com,R} + K_S\, V_{com,S}$, where K_R and K_S are:

$$\begin{cases} K_R = \dfrac{Agg_1(1+\lambda)}{Agg_1(1+\lambda)+g\left(\dfrac{2\pi r}{n}-d\right)+g_1(1+\alpha)(d-\rho)} \\ K_S = \dfrac{(d-\rho)g_1}{Agg_1(1+\lambda)+g\left(\dfrac{2\pi r}{n}-d\right)+g_1(1+\alpha)(d-\rho)} \end{cases} \tag{17}$$

λ is the ratio between end-winding C_{wr} and without end-winding C_{wr} which is usually less than 0.05. g and A are:

$$\begin{cases} A = C_{wr} = \dfrac{\varepsilon_{r1}(g_2\varepsilon_{r1} + g_{in}\varepsilon_{r2})(W' + 2\times h_W) + g_{in}\varepsilon_0\varepsilon_{r1}\varepsilon_{r2}(W - d)}{g_{in}(g_2\varepsilon_{r1} + g_{in}\varepsilon_{r2})} \\ g = g_1 + g_2 + \rho \end{cases} \quad (18)$$

Therefore, shaft voltage in DFIG is a function of different parameters such as: W, d, h_w, g_{in}, ε_r, ρ, g_1, g_2. Fig.10 (b and c) show the K_R and K_S versus variations of g_2 and d (λ=0.05, ρ=5mm, g_1=1mm, w′=150, W=120 mm, h_W=230 mm, g_{in}=2mm, ε_r=2.25). Fig.10.d and e show the K_R and K_S versus variations of ε_r and g_{in} (λ=0.05, ρ=5mm, g_1=1mm, w′=150mm, W=120mm, h_W=230 mm, d=50mm, g2=10mm).

According to the analysis:

- Majority of rotor side common mode voltage converts to shaft voltage (by factor of K_R which is near 1) while the stator side common mode voltage does not have a big effect on the shaft voltage. This fact should be mentioned as a key factor in shaft voltage mitigation techniques. The capacitive coupling between the rotor winding and rotor frame has a significant value compared with other capacitances. The major part of the common mode voltage will be placed across the shaft.
- With a variation of gap between winding and stator (g_2) and length of slot tooth (d), it is possible to control the shaft voltage but as it can be seen from Fig.10 (b and c), the effects of these factors are not so high. As shown in Fig.10 (d and e), the effects of the permittivity and thickness of the insulator in the rotor slots are very effective in shaft voltage reduction. In fact, the permittivity and the thickness of the insulator in the stator slots have less effect in reducing shaft voltage (Fig.3.a).

6. Conclusions

The capacitive coupling between rotor and stator winding is a key factor in shaft voltage generation in IG. Some parameters can change the capacitance such as: stator slot tooth, gap between slot tooth and winding, and height of slot tooth and air gap between rotor and stator. In a DFIG, the capacitive coupling between the rotor winding and rotor has a significant value compared with other capacitances. These parameters can be changed to achieve the lowest possible shaft voltage but the range of variation has to meet the electromechanical and thermal considerations. To reduce the shaft voltage, this analysis needs to be considered in design procedure for the induction generator structures.

7. Acknowledgment

The authors thank the Australian Research Council (ARC) for the financial support for this project through the ARC Discovery Grant DP0774497.

8. References

[1] J. M. Erdman, R. J. Kerkman, D. W. Schlegel, and G. L. Skibinski, "Effect of PWM inverters on AC motor bearing currents and shaft voltages," IEEE Transactions on Industry Applications, vol. 32, pp. 250-259, 1996.

[2] C. Mei, J. C. Balda, W. P. Waite, and K. Carr, "Minimization and cancellation of common-mode currents, shaft voltages and bearing currents for induction motor drives," PESC '03, IEEE 34th Annual, 2003.

[3] Jafar Adabi, Firuz Zare, Gerard Ledwich, Arindam Ghosh, “Leakage Current and Common Mode Voltage Issues in Modern AC Drive Systems”, AUPEC 2007, Perth, Australia, Dec 2007.

[4] Firuz Zare, “Modelling of Electric Motors for Electromagnetic Compatibility Analysis”, AUPEC 2006, Melbourne, Australia, Nov 2006.

[5] ABB Technical guide No.5 ‘bearing currents in modern AC Drive systems”, Helsinki, 1999

[6] Annette Muetze, Andreas Binder, “Techniques for Measurement of Parameters Related to Inverter-Induced Bearing Currents”, IEEE Transactions on Industry Applications, Vol. 43, No. 5, September/October 2007

[7] Annette Muetze, Andreas Binder, “Calculation of Influence of Insulated Bearings and Insulated Inner Bearing Seats on Circulating Bearing Currents in Machines of Inverter-Based Drive Systems”, Industry Applications, IEEE Transactions on, Vol. 42, No. 4, July/August 2006

[8] A. Muetze, A. Binder, “Calculation of motor capacitances for prediction of the voltage across the bearings in machines of inverter-based drive systems” , IEEE Transactions on Industry Applications, vol. 43, no. 3, pp. 665-672, June 2007

[9] S. Chen, T. A. Lipo, and D. Fitzgerald, “Source of induction motor bearing currents caused by PWM inverters” Energy Conversion, IEEE Transaction on, vol. 11, pp. 25-32, 1996.

[10] A.M.Garcia, D.G. Holmes, T.A. Lipo, “Reduction of Bearing Currents in Doubly Fed Induction Generators” Industry Applications Conference, 2006. 41st IAS Annual Meeting, Conference Record of the 2006 IEEE, Volume 1, pp. 84-89

[11] J.Adabi, F.Zare, A.Ghosh, R.Lorenz, “Analysis of Shaft Voltage in a Doubly-fed Induction Generator”, ICREPQ’09, Valencia, Spain, April 2009

[12] J.Adabi, F.Zare, “Analysis, Calculation and Reduction of Shaft Voltage in Induction Generators”, ICREPQ’09, Valencia, Spain, April 2009

[13] Matthew N.O.Sadiku, “Elements of Electromagnetics” third edition, New York, Oxford University Press, 2001

[14] ANSYS® Academic Research, Release 11.0, Help System, Electromagnetic Field Analysis Guide, ANSYS, Inc.

Figures:

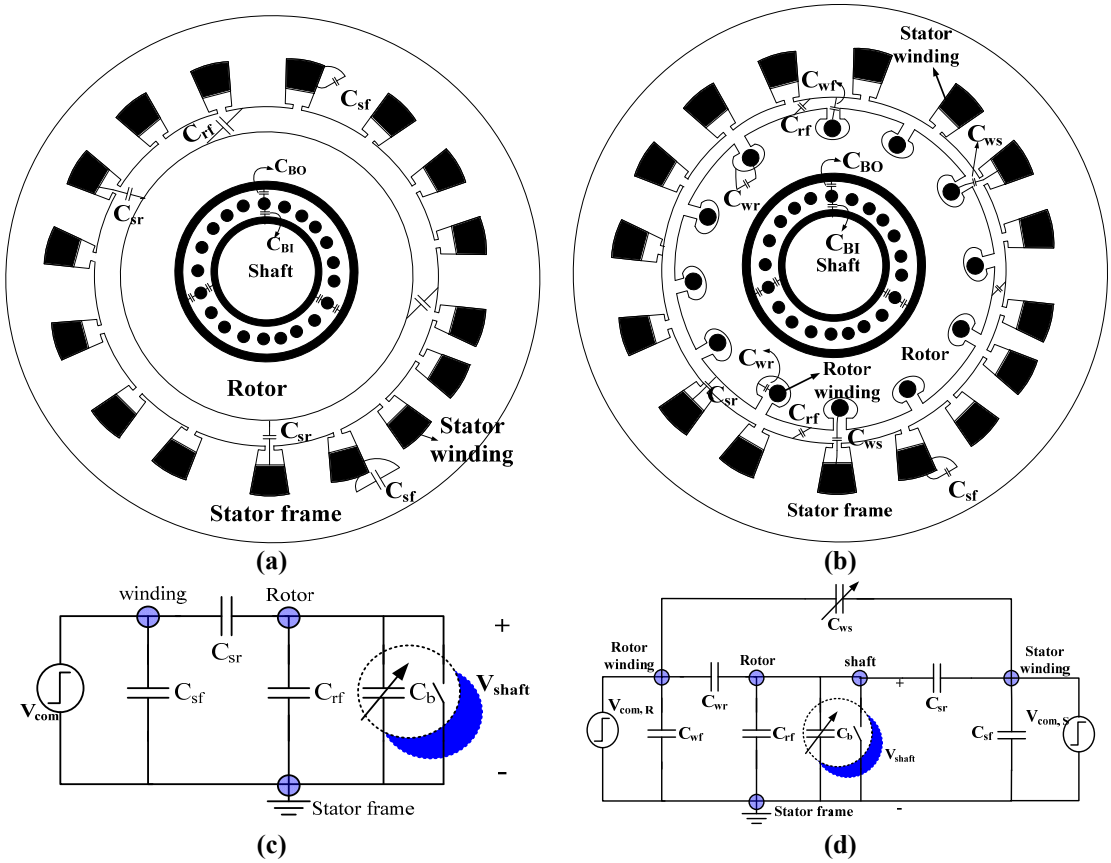

Fig.1. (a) Structure of an IG with different parasitic capacitive couplings (b) A view of a DFIG with different parasitic capacitive couplings with and high frequency model of (c) IG (d) DFIG

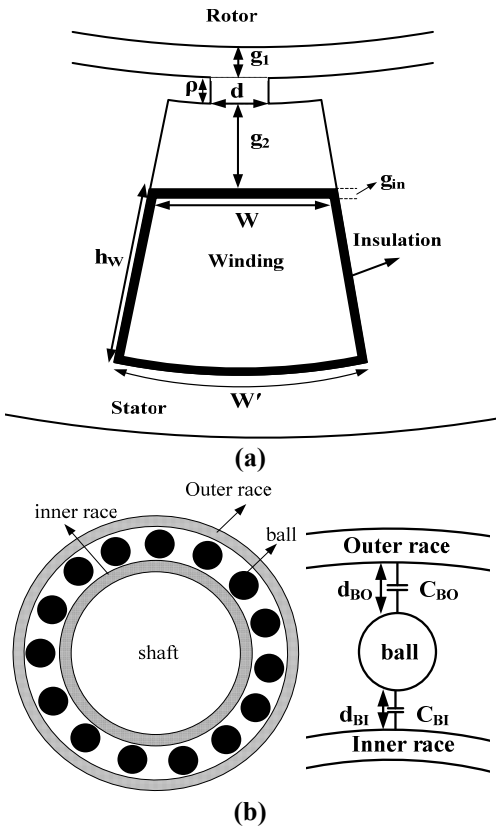

Fig.2. (a) A view stator slot and different design factors (b) ball bearings and shaft of a motor with a view of ball, outer and inner races and the capacitances

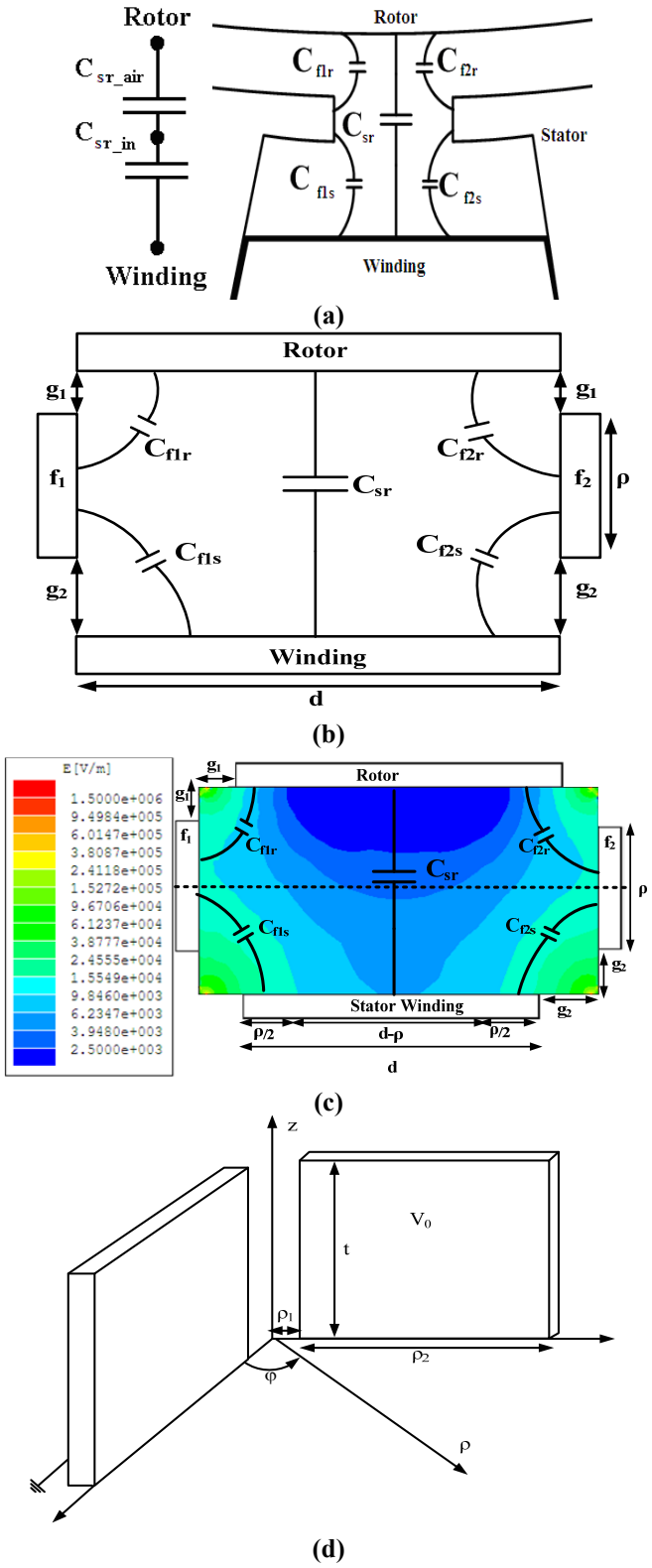

Fig.3. (a) capacitive couplings in a stator slot (b) a complete system model for calculation (c) simplified model with electric fields (d) two vertical surfaces

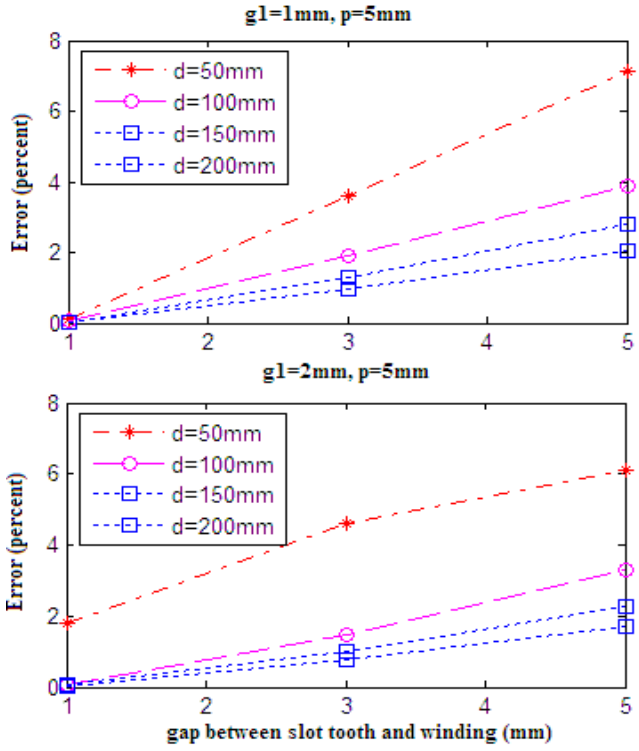

(a)

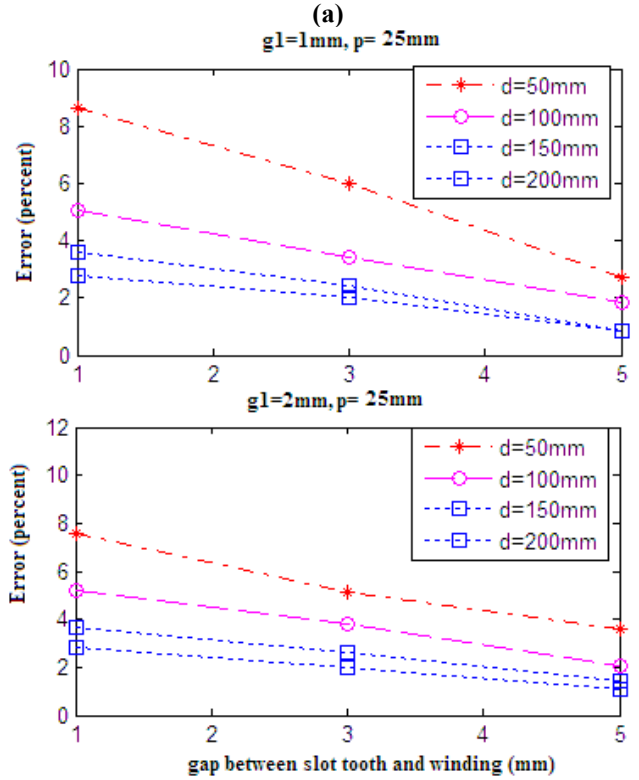

(b)

Fig.4. error between simulations and calculations of C_{sr} in a complete system model versus a variations of g_1 and g_2 (a) ρ=5mm (b) ρ=25mm

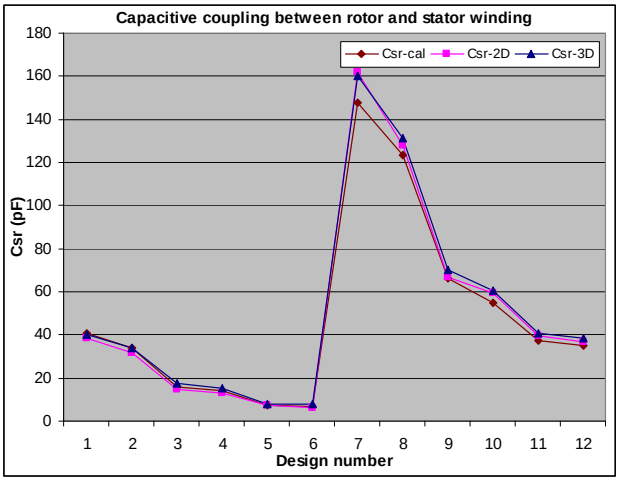

(a)

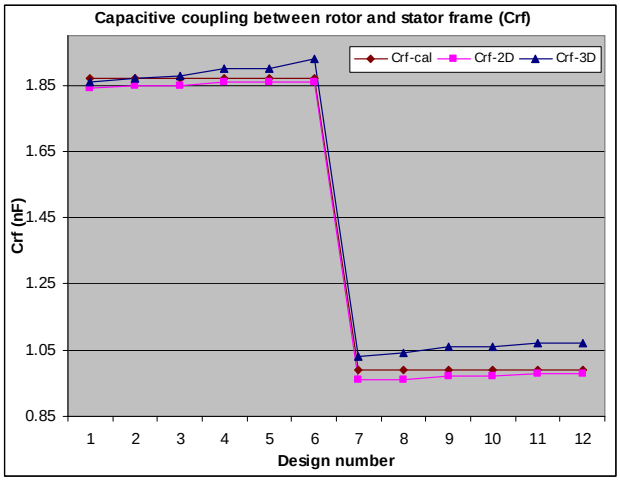

(b)

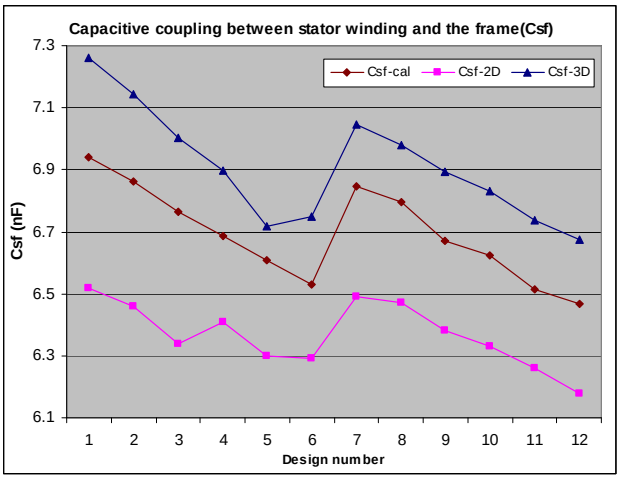

(c)

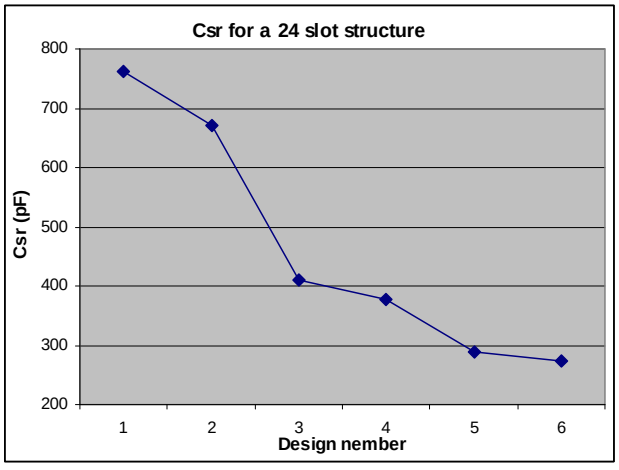

(d)

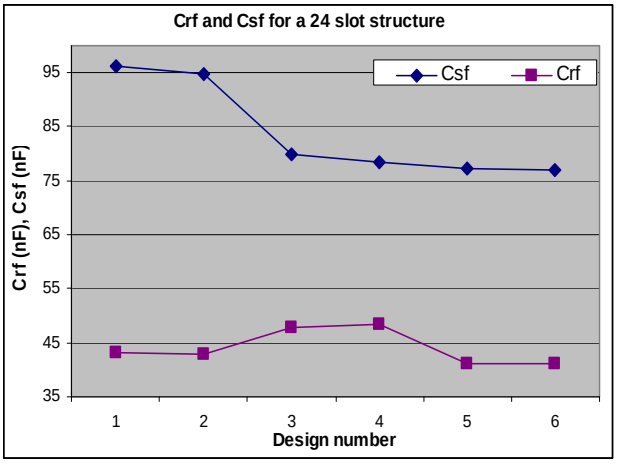

(e)

Fig.5. Calculated, 2-D, 3-D results in single stator slot for capacitive couplings (a) C_{sr} (b) C_{rf}(c) C_{sf} ; 3-D simulation results in a 24 slot IG for (d) C_{sr} (e) C_{rf} and C_{sf}

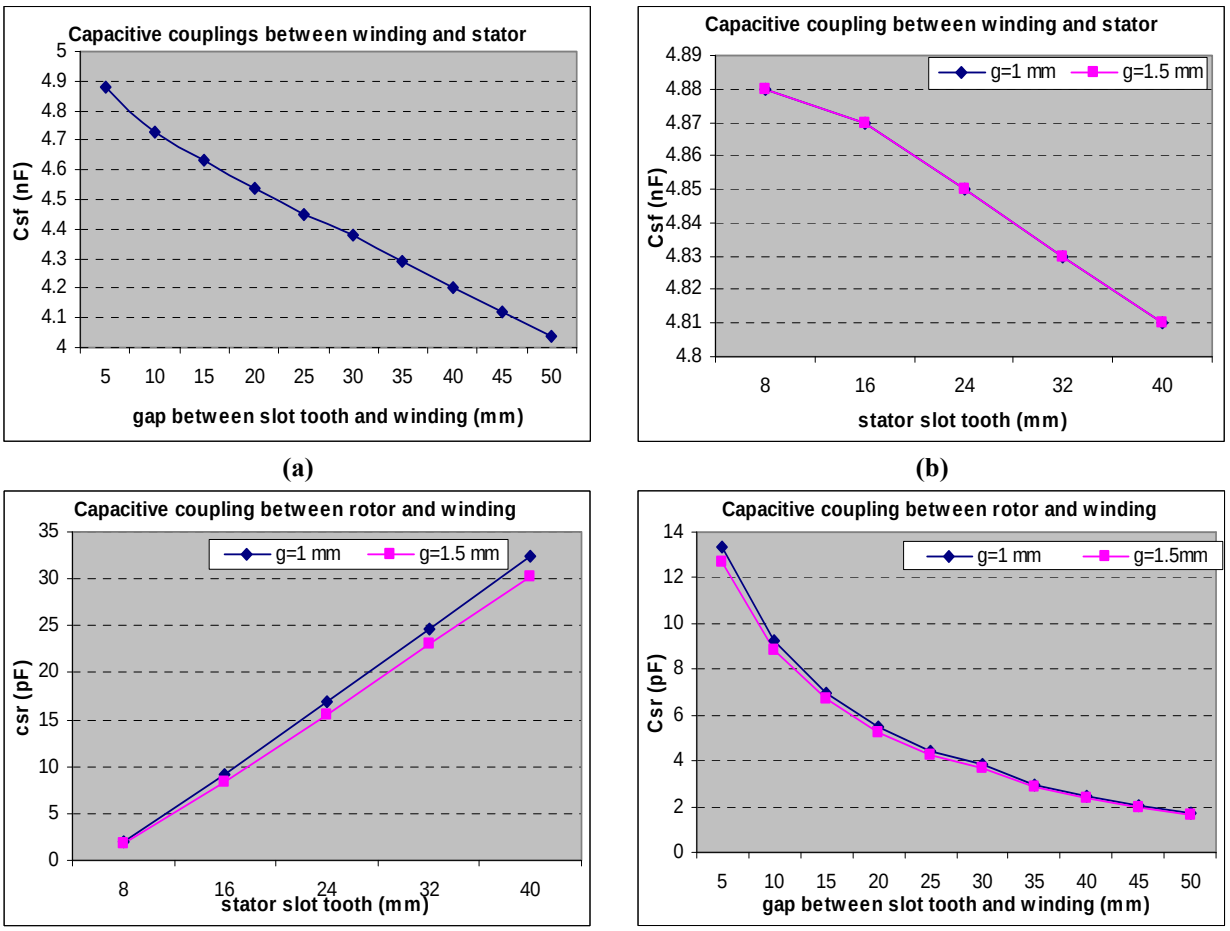

Fig.6. variation of C_{ws} versus: (a) the changes of g_2 (b) stator slot tooth and two different air gaps. variation of Cwr versus: (c) stator slot tooth (d) changes of g_2

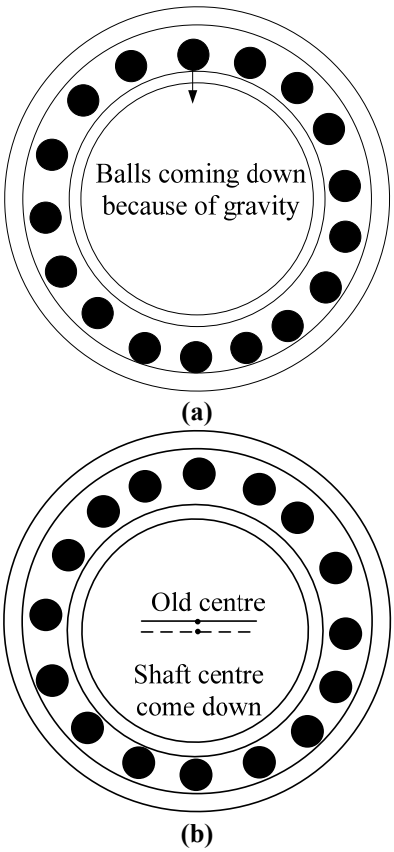

Fig.7. Asymmetric (a) ball positions (b) shaft position

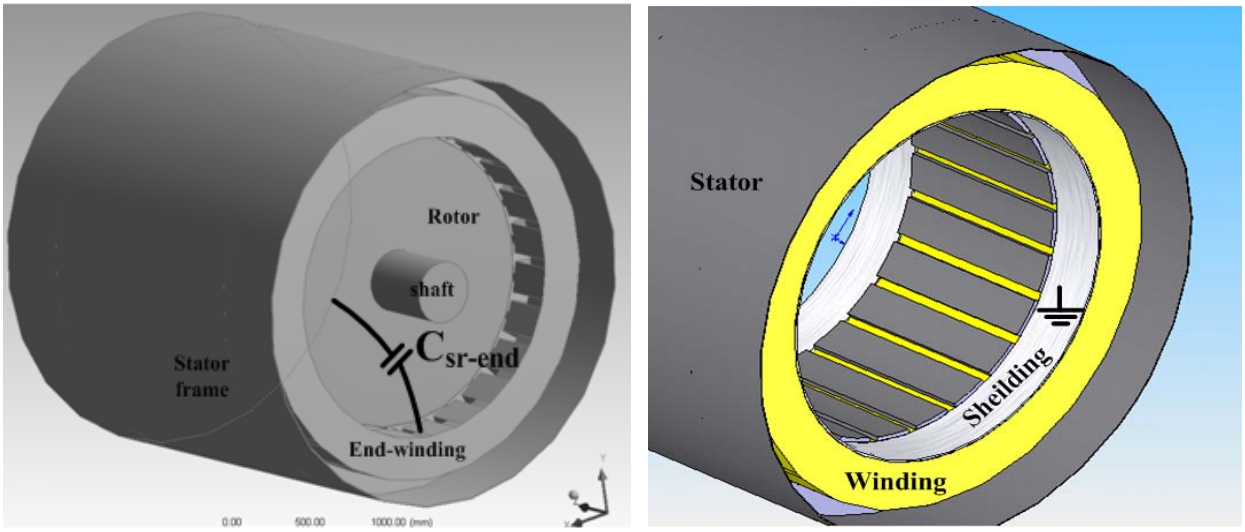

(a) (b)

Fig.8. view of (a) machine structure with end-winding (b) shielded end winding

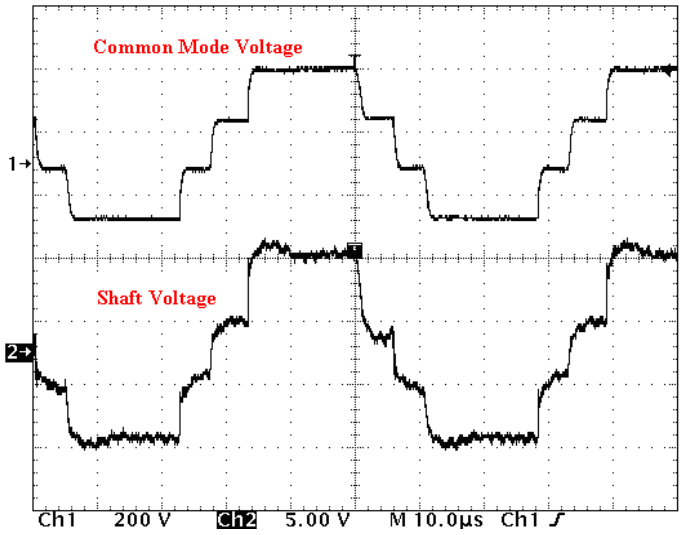

(a)

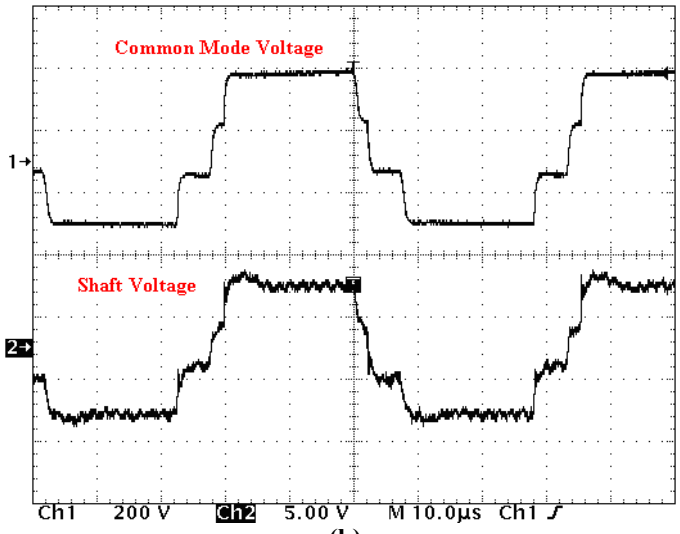

(b)

Fig.9 Experimental results: Common mode and shaft voltage waveforms (a) without shielded end winding (b) with shielded end winding

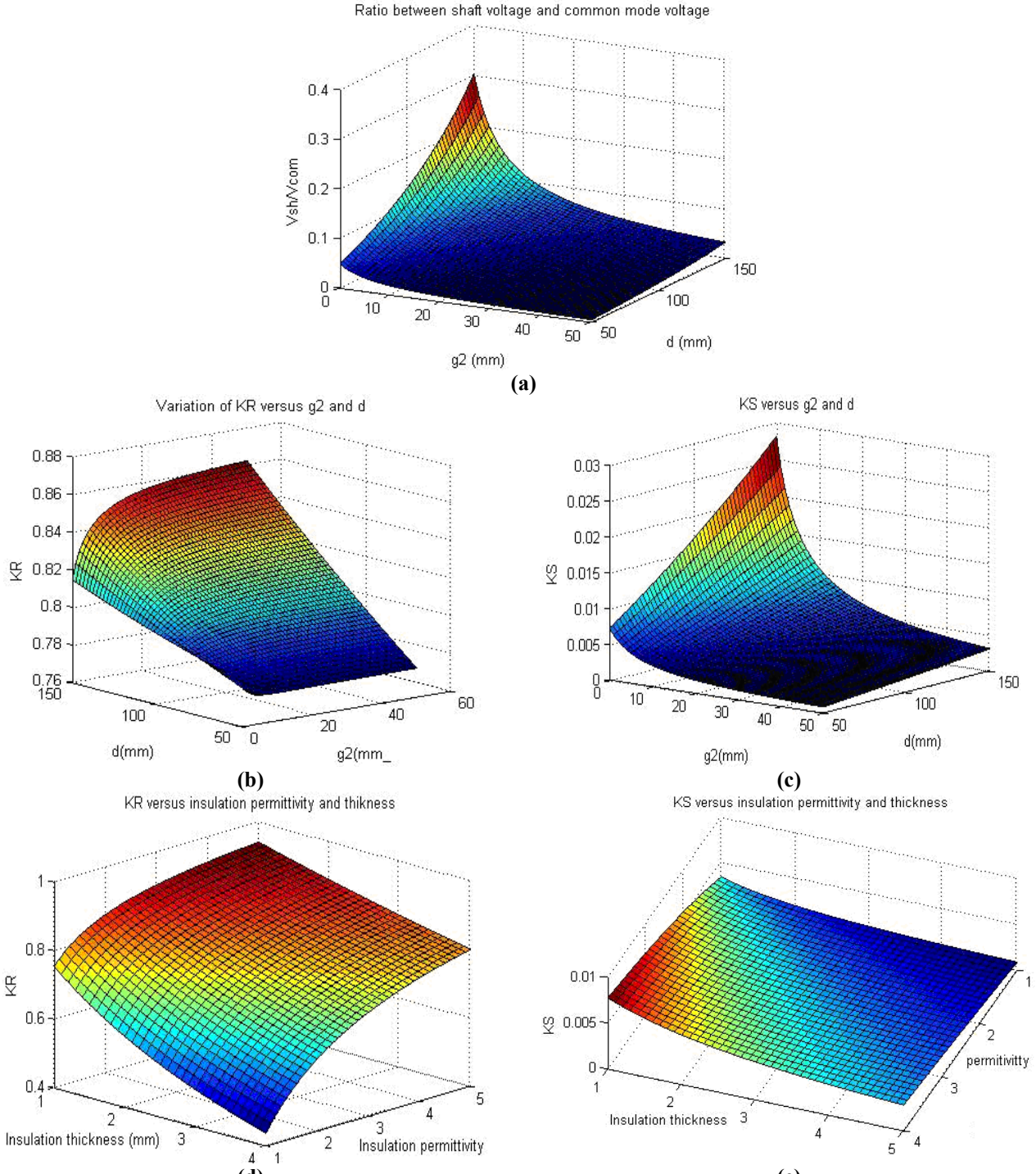

Fig.10. (a) V_{sh}/V_{com} versus d and g_2 (ρ=5 mm, x=1) ; (b) K_R versus g_2 and d (c) K_S versus g_2 and d (d) K_R versus ε_r and g_{in} (e) K_S versus ε_r and g_{in} in a doubly-fed induction generator